Monolayer Kr films adsorbed on BN

W. Li, P. Shrestha, and A. D. Migone

Department of Physics, Southern Illinois University-Carbondale, Carbondale, Illinois 62901

A. Marmier and C. Girardet

Universite de Franche-Comte, Faculte des Sciences et des Techniques, Laboratoire de Physique Moleculaire, La Bouloie-Route de Gray, 25030 Besancon CEDEX, France

We have conducted a detailed study of Kr films adsorbed on BN. We have performed adsorption-isotherm measurements and calculations for the potential energy of Kr atoms on the surface of BN. Both the experimental and the theoretical results are extensively compared to data for Kr on graphite, as well as to data for N_2 and CO on both BN and graphite. For N_2 and CO, the energy calculations found similar corrugations on BN and on graphite (these two molecular adsorbates do not discriminate between the B and N atoms on the BN substrate). This is not the case for Kr. The corrugation for Kr atoms (which do discriminate between B and N) is quite different on BN from what it is on graphite. Our adsorption isotherms indicate that a commensurate solid phase is present for Kr on BN. However, this commensurate solid exists only over a surprisingly narrow temperature interval of less than 5 K. Our experimental results are compared with those from previous studies of this system. We offer possible explanations for the differences observed and attempt to present a coherent picture of the experimental situation for this system. [S0163-1829(96)03226-2]

I. INTRODUCTION

Over the course of the past two decades a great deal of experimental and theoretical attention has been devoted to the study of films physisorbed on graphite.[1] The parallel development of sophisticated calculational tools and of more accurate experimental techniques has allowed researchers to correlate quite well the experimentally observed behavior of a film with detailed calculations of its interaction potential.

For most substrates (with a few notable exceptions, e.g., MgO),[2,3] the amount of information available lags well behind that which is available for graphite. In recent years there have been a number of studies of films adsorbed on BN;[4–9] information on this substrate continues to increase.[9] BN is an insulator that has the same structure as graphite, with 2% larger lattice parameters.[10]

We present the results of an investigation of Kr on BN that combines information obtained in adsorption isotherm experiments with theoretical calculations for the potential-energy surface of Kr on BN and with a determination of the most stable monolayer solid configuration of Kr at 0 K on this substrate. We compare our experimental results with those obtained in previous investigations of this system[11–13] and discuss the differences that exist between Kr on BN and Kr on graphite.[14–17] We use the results of the theoretical portion of this study to compare Kr films on BN with those of N_2 (Ref. 5) and CO (Ref. 6) on BN and on graphite.[18,19]

There have been three previous studies of Kr on BN.[11–13] Adsorption isotherms measured between 77 and 93 K, using a low density of data points (coverage intervals of ∼4% of a layer were employed), found no evidence of any phase transition in the first layer.[11] A second study simultaneously measured volumetric and dielectric isotherms at 78.3 K.[12] By contrast, this study found a fairly sharp solidification substep, near 0.16 Torr. A third study measured adsorption isotherms at 77.3, 78, and 90 K (Ref. 13) using a coverage interval of ∼1% of a layer. No substeps were found in this study.

On graphite, Kr, N_2, and CO form commensurate solids near monolayer completion. These three adsorbates have very similar monolayer phase diagrams.[20] At high coverages and temperatures, the commensurate solid melts to a reentrant fluid as the coverage is increased.[14–16] As the coverage increases further, the reentrant fluid solidifies to an incommensurate solid.[15,16] At low temperatures, the transition is directly from the commensurate to an incommensurate solid as the coverage is increased. Below the pure commensurate phase there is a coexistence region between the commensurate solid and a fluid phase.[14–16] A fluid phase is present at coverages below this two-phase coexistence region.[20]

Recent studies of N_2 (Ref. 5) and CO (Ref. 6) have found that, contrary to what occurs on graphite,[20] on BN these two adsorbates behave differently from Kr on BN. Both N_2 and CO exhibit the same sequence of phases on BN that they do on graphite.[5,6] (There are differences in the temperatures at which the phases appear on the two substrates, which reflect differences in substrate corrugation.)

II. EXPERIMENT

The experimental setup is the same one used in recent adsorption studies on BN performed in our laboratory.[4–7] It has been described in detail elsewhere.[21]

The Kr used in our measurements was research grade Matheson (purity 99.999%). The substrate used for all except one of the measurements reported here was BN type Alfa, manufactured by Johnson-Matthey. It has a surface area of 3 m^2/g. For comparison, one isotherm was measured on an
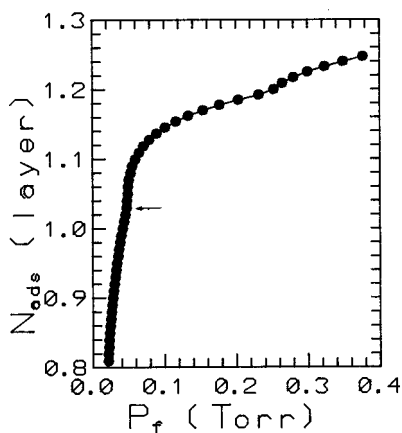
FIG. 1. N_2 adsorption isotherm on BN at 58 K. There are two features present in the data for this temperature: a lower-pressure sharp step, marked by the arrow, and a kink at higher coverages. The lower coverage feature corresponds to a commensurate solid plus fluid coexistence region, while the kink corresponds to the melting to a reentrant fluid.

Advanced Ceramics, type HCP, BN substrate; this powder has a surface area of 6.0 m^2/g.

Before being placed in the adsorption apparatus, the BN underwent a recently described cleaning treatment.[21] The powder was washed in methanol, filtered, and the resulting precipitate was placed in an oven at 900 °C under vacuum until the pressure reached below 5×10^{-6} Torr. This cleaning treatment has been shown to be effective in removing soluble borate contaminants from the BN.[21] Because soluble borates (boric acid and boric oxide) have very low vapor pressures even at 900 °C, these impurities cannot be removed by simply heating the powder to this or to lower temperature. Simple heating under vacuum has traditionally been the only cleaning method used for BN substrates.[11–13]

III. EXPERIMENTAL RESULTS

In order to characterize the BN substrate used in this study, we performed adsorption isotherms of Ar and of N_2 on the same powder that was used in the Kr measurements. The Ar measurements were conducted to determine whether the BN was free from soluble borate impurities.[21] The N_2 isotherm was measured to permit a comparison of the two adsorbates on exactly the same substrate.

In a previous study we had shown that the presence of soluble borate impurities in the BN leads to a broad compressibility peak in Ar adsorption isotherms.[21] The peak is due to Ar adsorption taking place on the impurities. For an Ar isotherm at 77.3 K the broad compressibility peak is centered near 6 Torr. We studied this region in detail and established that the substrate was free from impurities. No broad compressibility peak was found.

A N_2 adsorption isotherm was measured at 58 K; the data are displayed in Fig. 1. There are two features in the isotherm: a sharp substep and, at higher coverages, a kink. The sharp substep is due to the commensurate solid plus fluid coexistence region. The kink occurs when the pure commensurate solid melts to the reentrant fluid phase as the coverage is increased.[5]

We have measured 15 Kr adsorption isotherms on the same BN substrate for temperatures between 74 and 96 K. Some of our isotherms are presented in Fig. 2. There are four distinct regions present in the data in the range of coverages that we investigated (roughly, from $n = 0.75$ to above $n = 1.0$).

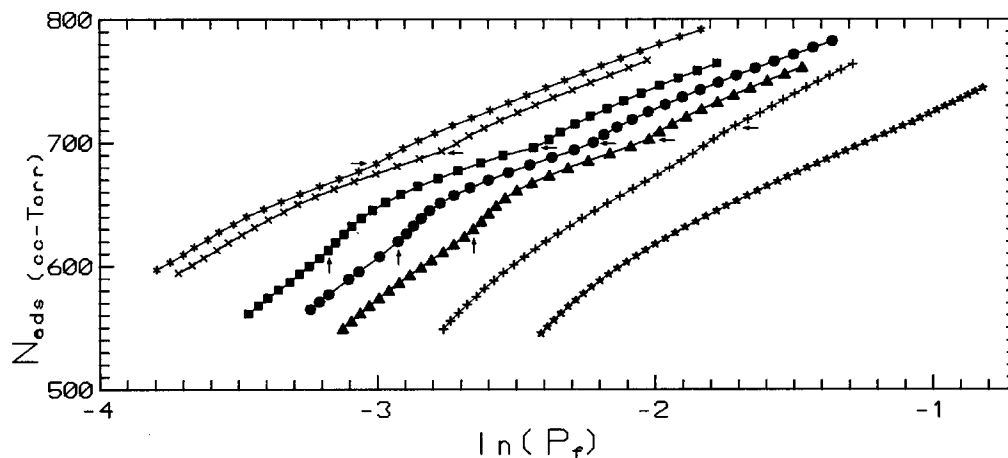(i) Between 74 and 82 K there is only a weak substep

FIG. 2. Adsorption isotherms for Kr on BN. The coverage (Y axis) is given in absolute units (1 cm^3 Torr at 273 K is equivalent to 3.5×10^{16} molecules). The X axis displays the $\log_{10}$ of the pressure (in Torr). Shown, from left to right, are data for $T = 78$ (*), 80 ($\times$), 83 ($\blacksquare$), 84 ($\bullet$), 85 ($\blacktriangle$), 90 (+), and 96 ($\star$). Only a weak substep or kink is present in the data measured below 83 K. For isotherms between 83 and 88 K there are two features in the data: at lower pressures there is a sharp step and at higher pressures there is a kink in the data. The isotherms measured in this narrow temperature interval (83–88 K) display characteristics very similar to those for N_2 or CO on BN (compare this figure to Fig. 1). The 90-K isotherm is characteristic of isotherms measured between 89 and 95 K: only a very weak substep is present in the data. For the 96-K isotherm there are no features present in the data, indicating that no transitions take place in the interval of pressures and coverages studied. (For the sake of clarity, the two highest temperature isotherms shown have been displaced along the X axis to lower values: the 90-K isotherm by one decade and the 96-K isotherm by 1.1 decades.) Horizontal arrows mark the position of the weak substep; vertical arrows mark the position of the low-coverage substep present between 83 and 88 K.
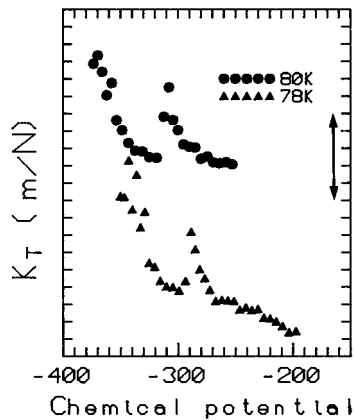
FIG. 3. Isothermal compressibility characteristic of adsorption isotherms measured between 74 and 82 K. The compressibility is shown for $T = 78$ and 80 K. The weak substep appears as a broad isothermal compressibility peak. The compressibility is displayed as a function of the chemical potential of the adsorbed gas (relative to the bulk chemical potential at the isotherm temperature). The data have been displaced along the Y axis for the sake of clarity. The double-headed arrow corresponds to an isothermal compressibility interval of 20 m/N.

present in the isotherms. This indicates there is a single transition occurring in the film as a function of increasing coverage at these temperatures. While it is difficult to estimate the coverage difference for this feature (because the step is not vertical), it certainly does not exceed 0.04 layers.

(ii) For isotherms between 83 and 88 K there are two features present: a sharp substep (occurring at coverages below those of the broad substep present for the lower-temperature isotherms) and a broader substep, at higher coverages. Isotherms in this temperature range display a sequence of features similar to that present for N_2 on BN, shown in Fig. 1.

(iii) For isotherms measured between 90 and 95 K only a single, broad, higher-coverage substep is present in the data.
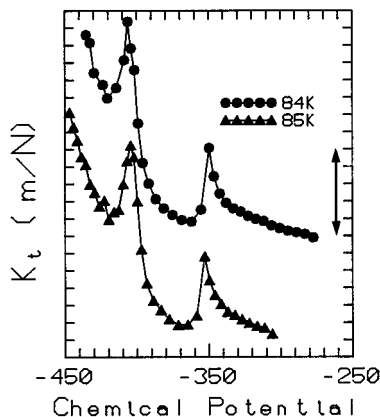

FIG. 4. Isothermal compressibility for adsorption isotherms at 84 and 85 K. The low-pressure sharp substep appears as a sharp isothermal compressibility peak, while the kink appears as a smaller peak. The compressibility corresponds well to that measured for N_2 at 58 K (see Fig. 1). The double-headed arrow corresponds to a isothermal compressibility interval of 25 m/N.
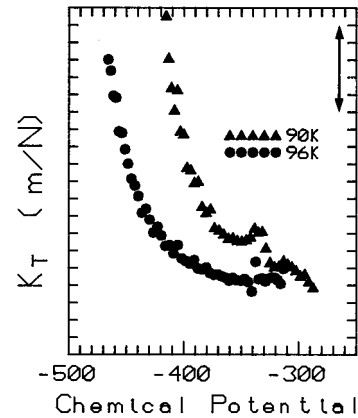

FIG. 5. Isothermal compressibility corresponding to adsorption isotherms at 90 and 96 K. The very weak substep present in the 90-K isotherm appears as a weak and broad isothermal compressibility peak. There are no compressibility peaks in the data corresponding to the 96 K isotherm. The double-headed arrow corresponds to 25 m/N.

This feature appears at increasingly higher coverages as the temperature of the isotherms is increased.

(iv) Finally, for the highest temperature studied, 96 K, there are no substeps present in the isotherm data, indicating the absence of transitions at this temperature in the coverage interval studied.

We have obtained the isothermal compressibility of the Kr films from the adsorption isotherm data. Selected isothermal compressibility traces, corresponding to the different regions, are displayed in Figs. 3–5. For temperatures between 74 and 82 K (Fig. 3) a single broad isothermal compressibility peak is present in the data. It has a peak height of approximately 15–20 m/N. For temperatures between 83 and 88 K (Fig. 4) there are two compressibility peaks present. The lower-pressure sharper peak is approximately a factor of 2 larger than the higher-coverage peak; this sharper peak has a height between 30 and 40 m/N. Above 88 K (Fig. 5) a single very weak peak is present in the data; its height is on the order of 6 m/N. No isothermal compressibility peaks are present in the 96-K isotherm (Fig. 5), the highest temperature studied.

In addition to the data measured on the 3.0 m^2/g BN powder on which most of the measurements were made, we investigated the effect of substrate quality by measuring one adsorption isotherm at 74 K on a sample of BN, type HCP, manufactured by Advanced Ceramics, with a specific surface area of 6.0 m^2/g. This sample of BN was subjected to the same cleaning treatment as that undergone by the BN powder used in the rest of the measurements. While the broad substep present at 74 K is still resolvable for the larger specific area BN sample, it appears as a weaker signature on this sample. This indicates that the weak isotherm substep for Kr on BN is sensitive to the quality of the substrate.

IV. CALCULATIONS

Prior to the work discussed below, there had been one theoretical study that attempted to determine the corrugation in the potential energy for rare gases on BN.[4] In that study,
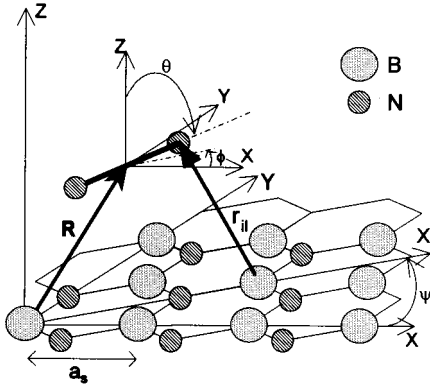
FIG. 6. Geometry of the adsorbate-substrate system. a_s is the lattice parameter, equal to 2.46 Å for graphite and 2.51 Å for BN. The angle ψ between X and X' is equal to $\pi/6$ on the figure.

each one of the B and N atoms in the substrate were replaced by the same ''effective atom'' of BN. As we shall show, important information is lost by making that simplifying assumption.

In this section we first present, a detailed discussion of the interaction potential used. We then proceed to calculate potential-energy surfaces for single atoms of rare gases and single molecules of N_2 and CO on BN. Finally, we calculate the most stable monolayer structures at 0 K for rare gases on BN and compare the energies for commensurate and incom-

mensurate structures for N_2 and CO on this substrate.

A. Interaction potentials

The interactions are separated into adsorbate-adsorbate and adsorbate-substrate terms

$$V(R,\Omega) = V_{AA} + V_{AS}. \tag{1}$$

Both the adsorbate and the substrate are taken to be underformable, so that V depends only on $\mathbf{R}$, the position of the center of mass, and on Ω, the orientation of the adspecies (see Fig. 6).

The dominant interactions in V_{AA} are the quantum contributions, which are treated in the usual form with an atom-atom Lennard-Jones potential

$$\nu_{ij}^Q = -4\varepsilon_{ij} \sum_{k=6,12} (-1)^{k/2} \left(\frac{\sigma_{ij}}{r_{ij}}\right)^k, \tag{2}$$

where i and j label two rare gases as well as two atoms belonging to two different molecules. The sets (ϵ,σ) for the various pairs, taken from the literature,[22–25] are given in Table I.

For N_2 and CO the quantum interactions are supplemented by multipolar electrostatic potentials, which are represented by interactions between distributed multipolar moments (to include the effect of the finite extent of the electronic cloud). For N_2 a three-point-charge distribution

TABLE I. Lennard-Jones potential parameters.

Interactions	Atomic pairs	ϵ_x [a]	σ_x [a]	ϵ_Y [b]	σ_Y [b]
substrate-substrate	B-B	1.92	4.32	2.02	3.84
	C-C	2.29	3.83	2.42	3.40
	N-N	2.38	3.52	3.52	3.12
adsorbate-adsorbate	Ar-Ar	10.41	3.45	10.41	3.45
	Kr-Kr	15.49	3.66	15.59	3.65
	N-N	2.38	3.52	3.11	3.32
	C-C	2.29	3.83	3.05	3.88
	O-O	2.09	3.38	4.99	2.88
	C-O	2.19	3.60	3.88	3.13
substrate-adsorbate	B-Ar	4.46	3.89	4.59	3.64
	C-Ar	4.88	3.64	5.03	3.42
	N-Ar	4.98	3.48	5.12	3.28
	B-Kr	5.45	3.99	5.60	3.75
	C-Kr	5.95	3.74	6.10	3.53
	N-Kr	6.08	3.58	6.25	3.43
	B-N	2.14	3.92	2.51	3.58
	C-N	2.34	3.67	2.65	3.36
	N-N	2.38	3.52	2.80	3.22
	B-C	2.09	4.02	2.48	3.61
	B-O	2.00	3.85	3.16	3.36
	C-C	2.39	3.83	2.71	3.39
	C-O	2.19	3.60	3.46	3.14
	N-C	2.34	3.67	2.77	3.25
	N-O	2.23	3.45	3.53	8.00

[a]Parameters calculated by using the usual combination rules from the data of Ref. 22, except for rare gases (Ref. 23).

[b]For graphite, values given by (Ref. 24) and for BN scaled from the parameters of Ref. 24.

TABLE II. Distributed multipole moment values (a.u.).[a]

		N/C	N/O	Bond site
N_2	$M^{(0)}$	−0.405	−0.405	0.0810
	$M^{(0)}$	0.5655	0.2994	−0.865
CO	$M^{(1)}$	1.057	−0.414	−0.287
	$M^{(2)}$	−0.236	0.130	0.763

[a]The multipoles $M^{(n)}$ are located on the atomic site and at the middle of the molecular bond.

model[26] appears to be convenient, while for CO distributed charges, dipoles, and quadrupoles are required[27] to ensure the convergence of the multipolar series expansion. We can write the general expression for the electrostatic contribution as

$$\nu_{ij}^E = \sum_{n,m} M_i^{(m)} T_{ij}^{(m+n)}(r_{ij}) M_j^{(n)}, \qquad (3)$$

where $M_i^{(m)}$ defines the mth point multipole at the ith site in the molecule and $T_{ij}^{(m+n)}$ is the usual action tensor of the electrostatic fields. The values of $M^{(m,n)}$ are given in Table II. The adsorbate-adsorbate potential V_{AA} is obtained after summing Eqs. (2) and (3) over the molecular sites (atoms) and over the adsorbate molecules.

The molecule-substrate interactions V_{AS} are based on a modified Lennard-Jones form which accounts for the distortion of the electronic distribution in the BN substrate in a manner similar to that of the model developed by Carlos and Cole for graphite.[28] This atom-atom potential between an adsorbate and a substrate atom is written as

$$\nu_{ij}^{MQ} = 4\varepsilon_{il} \sum_{k=6,12} (-1)^{k/2} \left(\frac{\sigma_{il}}{r_{il}} \right)^k [1 + \gamma_k - a_k \gamma_k \cos^2(n, r_{il}^0)], \qquad (4)$$

where γ_6 and γ_{12} describe the attractive and repulsive anisotropies in the polarizability of the BN substrate, $a_6 = \frac{3}{2}$ and $a_{12} = \frac{6}{5}$ are numerical coefficients, and $\mathbf{n}$ is the unit vector normal to the surface. Unlike the case for graphite, the information on the interaction parameters on BN is very poor. We are thus left just with considering two different sets of parameters for Eq. (4). In Table I, the parameters denoted by the subindex X were obtained using combination rules of homogeneous atomic pairs given in the literature. The parameters denoted by the subindex Y were obtained by correcting the (ϵ, σ) values for an atomic pair by effective bulk scale factors. This is done in order to account for the presence of the surrounding solid. The scale factors tend to slightly increase the ϵ parameter and significantly decrease the Lennard-Jones diameter σ relative to the unscaled values. When these scale factors are used for the graphite surface, they allow the molecule-graphite holding potential to fit very well the adsorption characteristics (isosteric heat of adsorption, molecule-surface distance, etc.). The parameters γ_6 and γ_{12} are not known for BN, so we assumed that they have the same values as they do for graphite, i.e., $\gamma_6 \simeq 0.4$ and $\gamma_{12} \simeq -1.05$.

In addition to the contribution to V_{AS} given in Eq. (4), Vernov and Steele[29] proposed that bonding in graphite gives rise to aspherical atomic charge distributions that are the source of electrostatic fields exhibiting spatial gradients. They considered the presence of an axially symmetric quadrupole moment at each carbon site, associated with sp^2 hybridization. We expect a similar effect on the BN surface with, however, a significantly different behavior due to the insulating nature of this substrate when compared to graphite. We write the electrostatic contribution to V_{AS}, between the quadrupole moments $M_l^{(2)}$ on B and N and the multipolar moments of the admolecule as

$$\nu_{il}^E = \sum_m M_i^{(m)} T_{il}^{(m+2)}(r_{il}) M_l^{(2)}. \qquad (5)$$

The quadrupolar tensor $M_l^{(2)}$ is diagonal in the surface frame and a single component, usually $(M_l^{(2)})_{zz}$, needs to be determined. For a pure quadrupolar charge distribution aligned along the normal to the surface, the calculated effective value for carbon[30] is about 1.0×10^{-26} esu cm^2 (0.753 a.u.). For boron and nitrogen atoms with, respectively, unoccupied (B) and twofold occupied (N) p_z Hückel orbitals, an estimate of $(M_l^{(2)})_{zz}$ leads to values 0 and 2.0×10^{-26} esu cm^2 (1.487 a.u.). To account for the inaccuracy of this determination, we vary these values. The adsorbate-substrate interactions V_{AS} are thus the sum over the substrate and adsorbate sites of Eqs. (4) and (5).

Additional interactions (namely, substrate mediated interactions and electrostatic image effects) were considered in preliminary calculations, but were subsequently dropped. These additional terms do not change in an appreciable way any of the conclusions that will be obtained. They result in energy corrections of less than 10% in the magnitude of the adsorption energy, without changing the equilibrium adsorbate sites. These changes are not significant, given the accuracy of the dominant contributions to the interaction potential. Moreover, recent simulations by Hansen and Bruch[31] on N_2 films adsorbed on graphite conclude that the calculated transition temperatures are brought into closer agreement with experiment if substrate-mediated interactions are suppressed in the calculations.

To summarize, the potential for the molecule or atom-BN interactions is similar to that extensively discussed for graphite, with two main differences. In the quantum contributions, the B and N atoms are clearly discriminated by the (ϵ, σ) from either gas or bulk effective values (the substrate anisotropy of the polarizability is considered to be kept unchanged with respect to graphite, since it is mainly a result of the sp^2 hybridization in both substrates). In the electrostatic contribution, the presence of different quadrupole moments on B and N introduces another source of discrimination between the two substrate atoms. These differences are expected to be of fundamental importance in interpreting the monolayer structures formed on graphite and on BN.

B. Potential-energy surfaces for a single admolecule on the substrate

The axes and angles that describe the position and orientations of the adsorbate molecule and of the substrate are

TABLE III. Comparison of the adsorption energies (meV) and corrugations (meV) for rare gas and diatomic molecules adsorbed on BN and graphite. $E_{C,B,N,S,M}$ correspond, respectively, to carbon, boron, nitrogen, saddle point, and minimum adsorption energies and $\Delta E_{C,V}$ describe the corrugation above the surface and along equilibrium valley. The values in parentheses are associated to dispersion-repulsion contributions only (i.e., disregarding electrostatic terms).

		E_C	E_B	E_N	E_S	Equilibrium site[a]	E_M	ΔE_C	ΔE_V
Ar	BN		-83.5	-88.6	-88.6	(0.5,0.29)	-92.1	8.6	3.4
	Gr	-94.2			-95.0	(0.5,0.29)	-101.5	7.3	6.5
Kr	BN		-112.9	-117.9	-117.9	(0.5,0.29)	-122.1	9.2	4.2
	Gr	-123.4			-124.3	(0.5,0.29)	-131.3	7.8	7.0
N_2	BN		$-89.9(-89.3)$	$-91.2(-92.4)$	$-92.0(-92.6)$	(0.36,0.37)	$-95.7(-94.9)$	5.8(5.6)	3.7(2.3)
	Gr	$-96.2(-96.5)$			$-98.0(-98.7)$	(0.5,0.29)	$-100.9(-100.00)$	5.0(3.5)	2.9(1.3)
CO	BN		$-94.0(-92.7)$	$-94.4(-96.8)$	$-97.0(-96.8)$	(0.33,0.39)	$-102.4(-100.6)$	8.4(7.9)	5.4(3.8)
	Gr	$-103.5(-104.3)$			$-105.4(-107.0)$	(0.5,0.29)	$-110.7(-110.2)$	7.2(5.9)	5.3(3.2)

[b]The equilibrium position (0.50,0.29) in reduced units of a_s defines the hollow site; for the other values, equivalent positions are obtained from symmetry considerations (C_3 or C_6).

displayed in Fig. 6. The equilibrium geometry for a single admolecule (rare gas, N_2, or, CO) was determined by minimizing $V_{AS}(R,\Omega)$ for the two sets of interaction parameters X and Y of Table I. The results for the Y parameters are presented in Table III. Additional calculations with the X set of parameters were aborted because they yield results that are at variance with known facts: the adsorption energies calculated with the X parameters are nearly equal on graphite and on BN, a feature inconsistent with the available experimental data,[32] and these parameters lead to molecule-substrate distances that are larger than the commonly accepted values.[32]

In Table III we give for every case the adsorption energy at 0 K above the on-top sites (C, B, or N), the energy above the equilibrium site (at or close to the hexagon center), and the energy for the saddle points. Moreover, we give the values of the corrugation energies ΔE_c and ΔE_ν, which are defined as the difference between the maximum and the minimum energies experienced by the adsorbate when it moves laterally above the surface (ΔE_c) and when it moves along the equilibrium valley (ΔE_ν). The potential-energy surfaces for Kr and N_2 on graphite and BN are presented in Fig. 7.

1. Rare-gas atoms

In Table III we see that the center of the hollow site corresponds to the equilibrium position for Ar and Kr on both substrates. The atom-surface distances are 3.44 and 3.54 Å for these two rare gases on BN. The B and N sites are discriminated by about 5 meV; the N site is more stable than the B site, which appears to be more repulsive. The hollow site is clearly more stable than the on-top sites. The corrugation energies ΔE_c and ΔE_ν are, respectively, around 9 and 4 meV. There is an equilibrium path going from the hollow to the N site. As a result, the surface appears to have rather a C_3 symmetry for the rare-gas atoms [Fig. 7(a)].

On graphite, the rare-gas adsorption site is again the hollow site, with atom-surface distances slightly smaller—3.32 Å for Ar and 3.44 Å for Kr. The adsorption energy is about 10% larger than on BN. The corrugation ΔE_c is slightly smaller on graphite for both adsorbates, while ΔE_ν is larger

for both Ar and Kr on graphite than on BN. The other significant differences are that the equilibrium valley goes from the hollow site to the middle of the C-C bond and that on graphite the surface has C_6 symmetry for the rare-gas atoms [Fig. 7(b)].

2. Diatomic molecules

While the hollow site appears to be the most stable adsorption site for N_2 and CO on graphite, the equilibrium position is slightly shifted with respect to the hexagon center on BN. This shift is nearly the same for the two molecules, though the molecular axes are flatter for N_2 than for CO. For CO the tilt reaches about $10°–15°$ with respect to the surface. The adsorption energy on BN is smaller by 5% (N_2) and 8% (CO) than on graphite. The values for N_2 are closer to those obtained for Ar than for Kr, Kr has the largest adsorption energy among the four species. The molecule-surface distances are equal to 3.39 and 3.29 Å for N_2 on BN and graphite; similar values are obtained for CO, respectively 3.26 and 3.17 Å . The corrugation energies ΔE_c and ΔE_ν are similar for the two substrates, but they are larger for CO than for N_2.

The main difference between the diatomic molecules (N_2 and CO) and the rare gases is the lack of discrimination between B and N atoms as viewed by the diatomic molecules. Indeed, while the N atoms behave as saddle points along the equilibrium valley for Ar and Kr, the N_2 and CO molecules do not experience significant differences between the B and N sites. This feature is due to the effect of the electrostatic adsorbate-substrate interaction, which tends to increase the repulsive part of the potential with the N and to balance the discriminating influence of the Lennard-Jones part. The influence of this electrostatic interaction on the magnitude of the adsorption energy is weak, as can be seen in Table III by comparing the energy values with and without including the electrostatic contribution to the molecule-surface potential. However, it appears to be sufficient for the diatomic molecules to change appreciably the shape of the potential-energy surface on BN as compared to that on graphite [cf. Figs. 7(c) and 7(d)], due to the eccentricity of the molecular center of mass. Indeed, since three equivalent
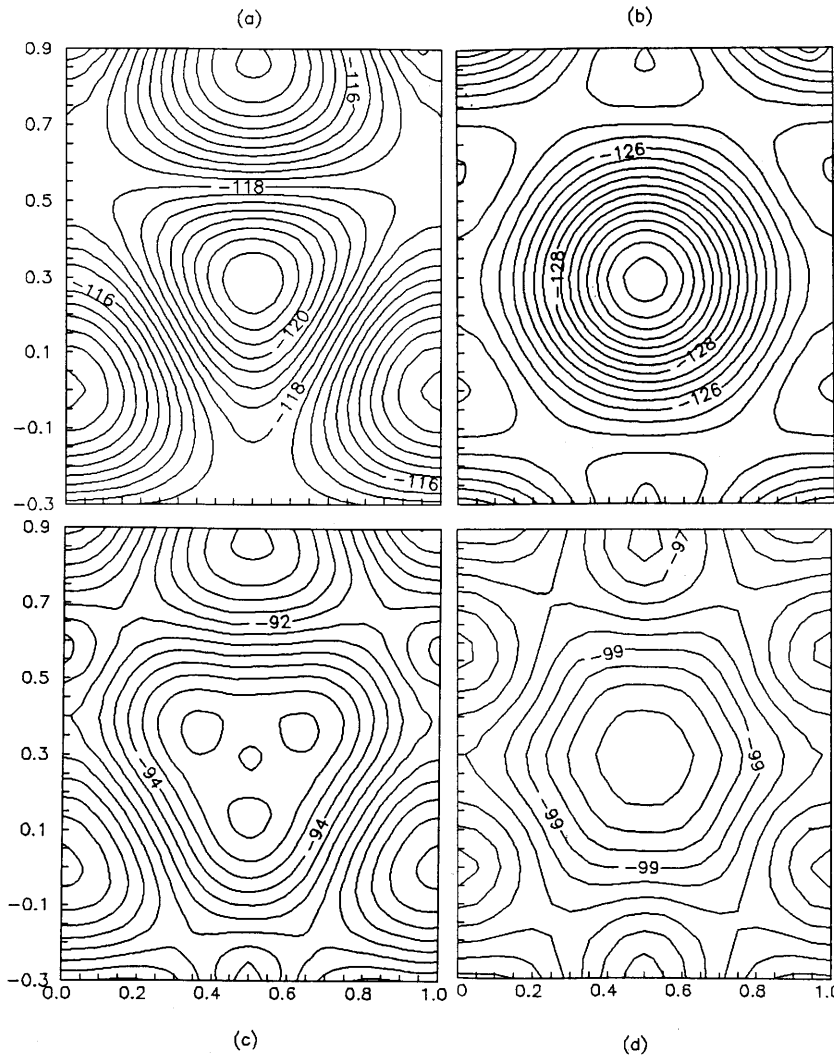
FIG. 7. Potential-energy surfaces for (a) Kr adsorbed on BN; (b) Kr adsorbed on graphite, (c) N_2 adsorbed on BN, and (d) N_2 adsorbed on graphite. All the energies are given in meV.

adsorption sites occur for N_2 on BN, the apparent symmetry is C_3. However, the N atoms are energy maxima, like the B atoms; the N_2 molecule is therefore hindered from freely moving outside the cup formed by the corners of the BN hexagon. This is to be contrasted with Kr on BN, for which the equilibrium valleys are along the N atom directions. Note that changing the values of the quadrupole moments of the substrate atoms (0.5×10^{-26} and 1.5×10^{-26} esu for B and N, respectively) decreases very slightly the discrimination and does not change the conclusions drawn here.

C. Monolayer geometries

1. Rare gases

To determine the most stable structures of the rare-gas layers adsorbed on graphite and on BN, we minimized the potential $V = V_{AA} + V_{AS}$ with respect to the positions of the centers of mass of the atoms. Among the infinite number of structures ranging from a low-order commensurate (LOC) phase to the incommensurate (floating) monolayer I, we selected layer geometries with lozenge-shaped unit cells, to be consistent with both the adsorbate's and substrate's atomic arrangements. We then applied two additional criteria.[33] First, lozenge-shaped unit cells are defined by two param-

eters: L, the side length, and ψ, the angle defining the rotation of the cells with respect to the X axis (see Fig. 6). Using the symmetry properties of the BN surface, one has $0 \leq \psi \leq \pi/6$. Moreover, assuming reasonable unit cell areas, one limits values of L to less than 20 Å . If a characterizes the substrate periodicity for the set (L, ψ), we can write $L = na$, where n is an integer number. Let there be m rare-gas atoms over the length L and let a_I be the incommensurate lattice parameter; then the registry misfit condition for the $(m:n, \psi)$ structure is written as

$$0.95 \leq (na/ma_I) \leq 1.05, \tag{6}$$

where the maximum and minimum values in Eq. (6) are chosen in such a way that the contraction or dilation of the structures considered do not yield a misfit larger than $\pm 5 \times 10^2$ when compared to the floating monolayer.

Such a criterion allows us to eliminate all the structures $(m:n, \psi)$ that are unrealistic and to distinguish the order of commensurability of the retained phases. (When $\psi = 0$ we will omit it in the structure nomenclature.)

The second criterion allows us the calculation of the average adsorption energy per adatom $\bar{E}_A = E_A / m^2$ at 0 K for the retained phases. A comparison of $\bar{E}_A$ for these structures,

TABLE IV. Comparison of the various structures for the monolayers. V_{AS}, V_{AA}, $\bar{E}_A$ are the equilibrium holding, lateral and average energies per atom or molecule.

	BN			Gr		
Ar	1:1($R30$)	2:3	I	1:1($R30$)	2.3	I
V_{AS}	-92.1	-87.9	-87.5	-101.5	-96.6	-96.1
V_{AA}	-24.9	-33.9	-34.6	-27.1	-32.1	-34.6
$\bar{E}_A$	-117.0	-121.8	-122.1	-128.6	-128.7	-130.7
Kr	1:1($R30$)	3:5	I	1:1($R30$)	3:5	I
V_{AS}	-122.1	-117.3	-117	-131.2	-125.8	-125.5
V_{AA}	-45.6	-50.0	-51.4	-48.3	-51.3	-51.4
$\bar{E}_A$	-167.7	-167.3	-168.4	-179.5	-177.1	-176.9
N_2 [a]	$3\times\sqrt{3}$		I	$3\times\sqrt{3}$		I
V_{AS}	$-95.7(-94.8)$		$-92.0(-92.4)$	$-100.9(-100.0)$		$-97.7(-98.1)$
V_{AA}	-28.5		-31.0	-29.9		-31.0
$\bar{E}_A$	$-124.2(-123.3)$		$-123.0(-123.4)$	$-130.8(-129.9)$		$-128.7(-129.2)$
CO [a]	$3\times\sqrt{3}$		I	$3\times\sqrt{3}$		I
V_{AS}	$-102.4(-100.6)$		$-97.7(-97.2)$	$-110.7(-110.2)$		$-106.1(-107.2)$
V_{AA}	-33.6		-36.2	-34.6		-36.2
$\bar{E}_A$	$-136.0(-134.2)$		$-133.9(-133.4)$	$-145.3(-144.8)$		$-142.3(-143.4)$

[a]Values in parentheses are associated to dispersion-repulsion terms only.

to find the one with the lowest energy, leads to the most stable geometry. This lowest-energy structure is expected to correspond to the actual structure of the monolayer.

For Ar adsorbed on BN, the lowest-order commensurate phase that satisfies the geometric criterion is the (2:3) structure, with four adsorbate atoms per unit cell. The other structures are clearly high-order commensurate (HOC) structures with more than 50 atoms per unit cell. This (2:3) low-order phase is compressed by 2%. The corresponding mean adsorption energy per atom is lower by 4.8 meV than for the $\sqrt{3}\times\sqrt{3}$ commensurate phase [i.e., the (1:1, $\pi/6$) structure]. However, the (2:3) structure is higher than the incommensurate phase by 0.3 meV (see Table IV). Similar results are obtained for Kr adsorbed on BN. The lowest-order commensurate structures are (3:5) and (5:8); they are nonrotated structures with, respectively, 9 and 25 atoms per unit cell and misfits equal to -2.8% and 1.3%. The other nonrotated and rotated structures are clearly HOC phases, with more than 40 atoms per unit cell. The (3:5) and (5:8) LOC phases have energies close to the $\sqrt{3}\times\sqrt{3}$ commensurate and to the incommensurate phases (Table IV), but the calculations show that this latter structure is slightly favored over the others.

On graphite, the stable Ar monolayer is the incommensurate phase, because the misfit of the (2:3) LOC structure corresponds to a compression of 4%, which is large enough to prevent the occurrence of such a geometry. The other nonrotated and rotated structures that are intermediate in energy are HOC. By contrast, graphite accommodates very well the $\sqrt{3}\times\sqrt{3}$ rotated commensurate Kr layer and also the (3:5) nonrotated geometry, which gives a very small misfit of -0.7%. The calculation of the mean adsorption energy per Kr atom nevertheless favors the stable $\sqrt{3}\times\sqrt{3}$ commensurate phase.

From the results presented in Table IV we thus see that

the rare-gas monolayers are in general incommensurate structures on BN and on graphite, except for Kr on graphite, which exhibits the (experimentally observed) commensurate geometry. The different behavior of Kr on the two substrates is the result of two effects. From a strictly geometric point of view, the graphite lattice parameter accommodates very well that of the Kr layer. From an energetic point of view, the graphite surface as viewed by the Kr atom is more corrugated than that of BN. The greater corrugation tends to trap the adatom in the potential cup with C_6 symmetry [cf. Fig. 7(b)]. The BN surface appears less corrugated. This surface allows the Kr atom to move easily along the equilibrium valleys formed by the hollow and N sites [Fig. 7(a)] and thus favors an incommensurate structure. A good basis for confidence in our calculations is the fact that they correctly yield, for Kr on graphite, the commensurate solid as the equilibrium phase, in agreement with what is experimentally observed.

2. Diatomic molecular monolayers

The presence of angular degrees of freedom prevents us from conducting the detailed analysis performed in the previous paragraphs. We limit our energy calculations to comparing the commensurate and incommensurate structures only. The conventional $3\times\sqrt{3}$ commensurate structure[34] with two orientationally inequivalent molecules per unit cell is always found to be the most stable structure (Table IV). The N_2 molecules are nearly flat above the BN surface, while the axes of the CO molecules are each slightly tilted by about 15° away from the surface and are mutually perpendicular ($\simeq 90\pm 5°$). The energy differences between the mean adsorption energy per molecule for the commensurate and incommensurate phases remain small, especially for N_2. It may be noted that these differences are still much

smaller when the electrostatic adsorbate-substrate interactions are disregarded; indeed, the relative stability of the *C* and *I* structures on BN can even be inverted. We should point out that while it is true that, in absolute values, the uncertainties in the interaction potentials used to appear to be of the same order as or larger than the differences calculated for the mean adsorption energy, the relative values of the differences calculated are much more accurate.

V. DISCUSSION

We compare our experimental results to previous reports for this system. The work by Dupont-Pavlovsky, Bockel, and Thomy[13] reports isotherms at 77.3, 78, and 90 K. At these temperature we only found a weak substep in the data (Fig. 2). While the study of Dupont-Pavlovsky, Bockel, and Thomy employed a high density of data points, the region they investigated in detail corresponds to coverages *higher* than those at which we found the weak substep.[13] It is quite probable that the region where the weak substep is present was missed in that study. The possibility of missing the weak substep is even stronger in the adsorption isotherm study of Regnier, Thomy, and Duval,[11] which utilized a coverage interval between data points too large to detect this rather broad feature.

In both the Dupont-Pavlovsky–Bockel–Thomy[13] and the Regnier–Thomy–Duval[11] studies the BN cleaning was limited only to heating the powder under vacuum. This method can leave soluble borate impurities on the substrate.[21] Impurities could be another possible source for the differences between our results and theirs.

The simultaneous volumetric and dielectric study by Laheurte *et al.*[12] reports on one isotherm at 78.3 K that is qualitatively similar to those we measured between 83 and 88 K, the only temperature interval where our isotherms have both a sharp substep and a kink. There is a kink present above the sharp substep in the data of Laheurte *et al.*,[12] even though this feature was neither noted nor discussed by the authors.

Some differences exist between our data and those of Laheurte *et al.*[12] We found no sharp substep in the isotherm at 78 K. The pressure at which we found the weak substep at 78 K is lower than that at which a sharp substep was measured in the combined dielectric and adsorption isotherm study (0.06 Torr in our study, 0.16 Torr in the dielectric study). The weak substep present in the Laheurte *et al.* study appears near 0.5 Torr,[12] at much higher pressures than the weak substep in our study. Possible explanations for the observed differences include the influence of the electric field (which is present in the dielectric experiment[12] but not in ours), which might alter the range over which the different phases are present, and the possibility of a cold spot in the dielectric experiment, which would result in a saturated vapor pressure corresponding to a lower temperature than that at which the BN powder is actually at.

The lack of structural information for Kr on BN restricts our ability to associate isotherm features with the phases present in the film. We are limited to compare isotherm and compressibility data and to guide us with the results of the calculations. For Kr on BN the low-temperature (i.e., between 74 and 82 K) adsorption isotherm and compressibility data are very similar to the data near the solidification for Ar
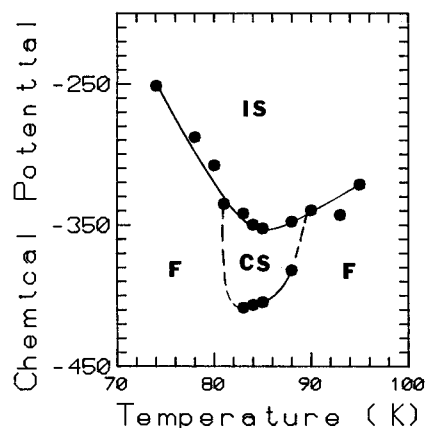

FIG. 8. Phase diagram for monolayer Kr on BN. The chemical potential (relative to the bulk chemical potential) is plotted as a function of temperature. The chemical potential difference is given in K. The phases proposed in this phase diagram are the following: IS, incommensurate solid; F, fluid; and CS, commensurate solid. The upper boundary of the commensurate solid region ends at either a reentrant fluid phase (which solidifies to an incommensurate solid at slightly higher coverages) or a commensurate-incommensurate transition.

and BN.[4] The calculations yield very similar results for the most stable monolayer solid for Ar and Kr on BN: in both cases it is the incommensurate solid. For both Ar and Kr on BN there is a small coverage interval involved in the transition and a relatively small compressibility peak suggestive of weakly first-order or continuous solidification.[4] We thus identify the weak substep between 74 and 82 K as corresponding to a solidification transition from a fluid to an incommensurate solid as the coverage is increased.

As noted before, the data for N_2 on BN and that for Kr on BN between 83 and 88 K are similar. We identify the lower-coverage sharp substep as indicative of a coexistence region between a fluid and a commensurate solid; this transition is first order. The existence of a very narrow temperature interval over which a commensurate phase exists is compatible with the results of our calculations. We note that all the calculations performed here have been conducted at 0 K and that the difference found between the average energies for the commensurate and incommensurate solid structures for Kr on BN is 0.7 out of 168 meV, or 0.4%. This is the smallest difference (both in absolute and percentual terms) between any $\sqrt{3} \times \sqrt{3}$ commensurate and incommensurate structure among those studied (see Table IV). Calculations for ionic and metallic substrates (which have larger corrugations than either BN or graphite[33]) find that finite-temperature contributions do not invert the relative stability of the solid phases. However, for Kr on BN the small corrugation and the small difference between the 0 K energies might result in the commensurate phase being favored over a narrow temperature interval at higher temperatures.

For temperatures between 83 and 88 K we interpret the broad substep present at higher coverages as being due to one of two possibilities. It corresponds either to a commensurate-incommensurate transition or to a pair of transitions that are too closely spaced for our experiment to resolve: first, from the pure commensurate to a reentrant

fluid phase, and then, at slightly higher coverages, a solidification of the reentrant fluid to an incommensurate solid (i.e., a sequence similar to that for CO, Kr, and N_2 on graphite).[20]

A plot of the chemical potential (relative to that of the bulk) vs temperature for the observed isotherm features, shown in Fig. 8, has a break in the slope of the line corresponding to the broad substep taking place near 83 K. This is an indication that between 83 and 88 K the broad substep corresponds to a different transition than that at lower temperatures.

The small substep present at temperatures above 88 K has smaller and broader compressibility peaks than the broad feature between 83 and 88 K. We identify it as corresponding to a weakly first-order or continuous solidification transition from a fluid to an incommensurate solid.

VI. CONCLUSION

Our adsorption isotherm and isothermal compressibility results show that Kr behaves differently on BN and on graphite and also differently from N_2 and CO on BN. Over the range of coverages and temperatures studied, the simplest interpretation for our data suggests that there is a very narrow temperature interval over which a commensurate solid phase is present for the Kr on BN system. The phase diagram corresponding to the region studied (in the chemical poten-

tial vs temperature plane) is presented in Fig. 8, which also constitutes a summary of our experimental findings. The narrow temperature width over which the commensurate solid is present for Kr on BN, together with the relatively broad features of the isotherm substeps for temperatures outside this narrow region, may help explain the absence of features reported in previous volumetric studies of this system.[11,13]

Our calculations show that N_2 and CO essentially do not discriminate between B and N atoms and, as a consequence, for them the corrugation on BN is very similar to that on graphite. Because the corrugation is essentially the same on both substrates, the sequence of phases (and hence the phase diagram) is the same for these two diatomic molecular adsorbates on BN and on graphite. By contrast, for Kr, the B and N atoms of the substrate look quite different. There are no electrostatic terms in the energy for Kr and the corrugation has a different symmetry on BN than on graphite. These differences help explain why CO and N_2 have the same sequence of phases on BN and on graphite, while Kr has a different phase diagram on these two substrates.

[1] See, for example, in *Phase Transition in Adsorbed Films 2*, Vol. 267 of *NATO Advanced Study Institute, Series B: Physics*, edited by H. Taub, G. Torzo, S. C. Fain, Jr., and H. J. Lauter (Plenum, New York, 1991).

[2] J. P. Coulomb, T. S. Sullivan, and O. E. Vilches, Phys. Rev. B **30**, 4753 (1982); J. Ma, D. L. Kingsbury, F. C. Liu, and O. E. Vilches, Phys. Rev. Lett. **61**, 2348 (1988); D. Degenhardt, H. J. Lauter, and R. Hansel, Jpn. J. Appl. Phys. Suppl. **26**, 341 (1987); J. L. Jordan, J. P. McTague, J. B. Hastings, and L. Passell, Surf. Sci. **150**, L82 (1985); see also J. P. Coulomb, in *Phase Transitions in Adsorbed Films 2* (Ref. 1), p. 113.

[3] A. Lakhlifi and C. Girardet, Surf. Sci. **241**, 400 (1991); C. Girardet and C. Girard, *ibid.* **201**, 278 (1988); C. Ramseyer, P. N. M. Hoang, and C. Girardet, *ibid.* **265**, 293 (1992).

[4] A. D. Migone, M. T. Alkhafaji, G. Vidali, and M. Karimi, Phys. Rev. B **47**, 6685 (1993).

[5] M. T. Alkhafaji, P. Shrestha, and A. D. Migone, Phys. Rev. B **50**, 11 088 (1994).

[6] J. M. Meldrim and A. D. Migone, Phys. Rev. B **51**, 4435 (1995).

[7] M. D. Evans, N. Patel, and N. S. Sullivan, J. Low Temp. Phys. **89**, 653 (1992).

[8] H. Wiechert, Bull. Am. Phys. Soc. **40**, 524, (1995); M. Willenbacher, E. Britten, E. Maus, and H. Wiechert (unpublished).

[9] A comprehensive summary of all work done on N_2 and CO on BN will appear in a review article by D. Marx and H. Wiechert, Adv. Chem. Phys. (to be published).

[10] R. W. G. Wyckoff, *Crystal Structures*, 2nd ed. (Interscience, New York, 1963), Vol. 1.

[11] J. Regnier, A. Thomy, and X. Duval, J. Colloid Interface Sci. **70**, 105 (1979).

[12] J. P. Laheurte, J. C. Noiray, M. Obadia, and J. P. Romagnan, Surf. Sci. **122**, 330 (1982).

[13] N. Dupont-Pavlovsky, C. Bockel, and A. Thomy, Surf. Sci. **160**, 12 (1985).

[14] R. M. Suter, N. J. Colella, and R. Gangwar, Phys. Rev. B **31**, 627 (1985).

[15] E. D. Specht, M. Sutton, R. J. Birgeneau, D. E. Moncton, and P. M. Horn, Phys. Rev. B **30**, 1589 (1984).

[16] P. W. Stephens, P. A. Heiney, R. A. Birgeneau, P. M. Horn, D. E. Moncton, and G. S. Brown, Phys. Rev. B **29**, 3512 (1984).

[17] R. Hoja and R. Marx, Phys. Rev. B **34**, 7823 (1986).

[18] M. H. W. Chan, A. D. Migone, K. D. Miner, and Z. R. Li, Phys. Rev. B **30**, 2681 (1984).

[19] Y. P. Feng and M. H. W. Chan, Phys. Rev. Lett. **64**, 2148 (1990); **71**, 3822 (1993).

[20] M. H. W. Chan, in *Phase Transitions in Adsorbed Films 2* (Ref. 1), p. 1.

[21] P. Shrestha, M. T. Alkhafaji, M. M. Lukowitz, G. Yang, and A. D. Migone, Langmuir **10**, 3244 (1994).

[22] M. A. Spackman, J. Chem. Phys. **85**, 6579 (1986).

[23] M. L. Klein and J. A. Venables, in *Rare Gas Solids* (Academic, London, 1977), Vol. II.

[24] W. A. Steele, J. Phys. (Paris) Colloq. **38**, C4-6 (1978).

[25] K. Mirsky, J. Chem. Phys. **46**, 445 (1980).

[26] C. S. Murty, K. Singer, M. L. Klein, and Y. R. Mac Donald, Mol. Phys. **41**, 1387 (1980).

[27] S. Picaud, P. N. M. Hoang, C. Girardet, A. Meredith, and A. J. Stone, Surf. Sci. **294**, 149 (1993).

[28] W. E. Carlos and M. W. Cole, Surf. Sci. **119**, 21 (1982).

[29] A. Vernov and W. A. Steele, Langmuir **8**, 155 (1992).

[30] F. Y. Hansen, L. W. Bruch, and S. E. Roosevelt, Phys. Rev. B **45**, 11 238 (1992).

[31] F. Y. Hansen and L. W. Bruch, Phys. Rev. B **51**, 2515 (1995).

[32] G. Vidali, G. Ihm, H. Y. Kim, and M. W. Cole, Surf. Sci. Rep. **12**, 133 (1991).

[33] C. Ramseyer, P. N. M. Hoang, and G. Girardet, Phys. Rev. B **49**, 2861 (1994).

[34] L. W. Bruch, J. Chem. Phys. **79**, 3148 (1983).